

# Revisiting ab-initio excited state forces from many-body Green's function formalism: approximations and benchmark

Rafael R. Del Grande\* and David A. Strubbe

Department of Physics, University of California, Merced, California, USA

(Dated: February 10, 2025)

Ab initio techniques for studying the optical and vibrational properties of materials are well-established, but only a few recent studies have focused on the interaction between excitons and atomic vibrations. In this paper, we revisit the excited state forces method, which integrates results from GW/BSE and DFPT calculations to determine the gradient of the excited state energy. We explore its technical aspects, including convergence and the quality of approximations used. We successfully apply this method to investigate self-trapped excitons in LiF. The excited state forces method provides valuable insights into ionic dynamics in the excited state and the microscopic mechanism of exciton self-trapping.

## I. INTRODUCTION

Light-induced changes in materials play an important role in photovoltaic degradation, Stokes shifts, exciton transport<sup>1,2</sup>, exciton localization<sup>3,4</sup>, charge separation, internal conversion<sup>5</sup>, and recombination. Light exposure in perovskites can induce its degradation<sup>6</sup>, phase transitions<sup>7</sup>, rotations of the organic cation<sup>8</sup>, and change of their lattice parameter<sup>9</sup>. In reference<sup>10</sup>, ultrafast experiments study the exciton coupling to coherent phonons in perovskites. In 2D materials, coherent phonons produced by light absorption were experimentally studied using ultrafast optical measurements<sup>11–15</sup>.

From the ab initio point of view, materials electronic structures are calculated using the GW method<sup>16</sup>, excitonic effects are studied using the Bethe-Salpeter Equation (BSE)<sup>17</sup>, and vibrational properties are studied using Density Functional Perturbation Theory (DFPT). Those methods are well established, although the combination of those two features is just being performed by recent works through the investigation of exciton-phonon coupling (EPC) influence on optical absorption and emission<sup>4,18–20,20–30</sup>. EPC redshifts the optical absorption at finite temperature<sup>2,20,26,29</sup>, increases the peaks linewidth<sup>2,21,22,26,29,31</sup> and makes new satellite peaks appear with energy higher than the main peak<sup>23</sup>. Exciton energy is redshifted due to the Fan-Midgal like exciton self-energy<sup>2,23</sup>. In references<sup>32,33</sup> exciton-exciton scattering mediated by phonons is included in *ab initio* theoretical Raman spectra calculations, while in reference<sup>34</sup> excitonic effects are included in second-order resonant Raman scattering calculations, which are important to understand Raman spectra of 2D TMDs<sup>35</sup>. In reference<sup>36</sup> it was shown that EPC is necessary to interpret experimental resonant inelastic x-ray scattering results. EPC is also essential to understand exciton relaxation pathways<sup>1,2,5,22</sup>. In references<sup>37,38</sup> the electron-hole interaction is modified by phonon screening in BSE calculations, which successfully describes the exciton binding energy dependence on temperature.

Interaction between excitons and phonons in *ab initio* has generally been treated via finite differences, also known as “frozen phonon” calculations, in which separate calculations are done on a series of structures with small atomic displacements, and the differences are used to approximate a derivative<sup>18,19,34,39</sup>. Performing the complete set of  $3N$  calculations ( $N$  is the number of atoms) is computationally prohibitive except for small systems<sup>40</sup> as BSE already scales as  $O(N^6)$ . A recent

linear-response cumulant approach to exciton-phonon coupling effects on absorption spectra<sup>41</sup> has been shown for a model system. In references<sup>38,42</sup> phonon effects are included in the kernel of the Bethe-Salpeter Equation, which increased the screening on the excitons and reduced their binding energy. In ref.<sup>22</sup> the authors derive the exciton-phonon coupling by writing the BSE hamiltonian on phonon-perturbed basis and project it in a perturbed basis where the BSE solutions are known. In references<sup>43,44</sup> a novel approach that combines solutions from the BSE and DFPT is presented, where the lattice distortions due to the EPC are obtained by minimizing the total energy composed as a sum of the excitation energy and the DFT energy in the harmonic approximation. This approach can be used to study excitons with polaronic character and is based on previous works that studied polarons<sup>45,46</sup>. Perebeinos et. al<sup>47</sup> used a similar approach combining tight binding and classical force fields to study EPC in carbon nanotubes. In Non-Adiabatic Molecular Dynamics (NAMD) simulations, excitonic effects can be added through solutions of GW-BSE calculations on ensembles of atomic trajectories<sup>5,48</sup>.

Besides the efforts of understanding EPC, there are just a few works that explore the molecular mechanisms of self-trapping of excitons using *ab initio* methods<sup>43,44,49–51</sup>. In those works the excitation energy is calculated as a function of the collective displacements of atoms and the exciton trapping is pointed out when the total energy surface reaches a minimum. As an example, we show the case for the CO molecule in figure 1, where we show the excited state energy of singlet and triplet excitons. As the CO molecule has just one degree of freedom then one can study easily the evolution of its excited state surfaces as a function of the CO bond length. For both singlet and triplet lowest energy excitons the minimum of the total energy leads to an increase of the CO bond length (see table I).

In more complex cases, one needs to find the minimum of the  $3(N - 1)$  dimensional excited state surface. One can use any relaxing algorithm that samples the exciton energy  $\Omega(R)$  in different configurations  $R$ , although this would demand several GW-BSE calculations. One useful information in this relaxation process is the gradient of the exciton energy with respect to the atomic coordinates  $\nabla_R \Omega(R)$ . This allows the use of algorithms like Steepest Descent (SD) and Conjugate Gradient (CG), highly used in *ab initio* simulation packages. In this paper, we focus on the gradient of the exciton energy

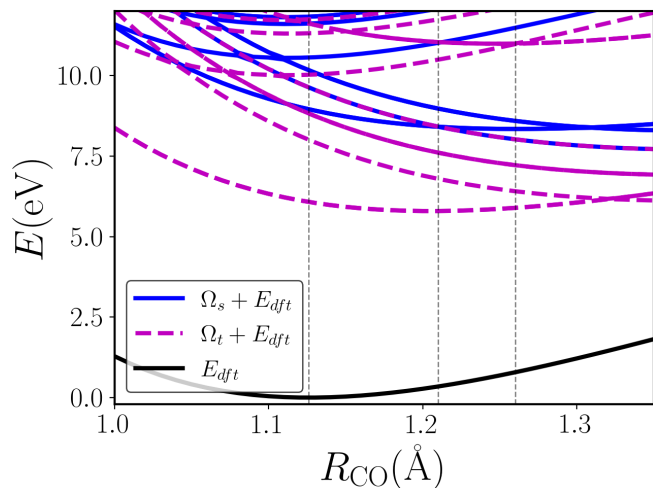


**Figure 1:** Ground state energy calculated at DFT level (black line), excited state energies calculated for singlet (blue line) and triplets (purple line). Vertical lines correspond to equilibrium distances 1.12 Å, 1.21 Å, and 1.26 Å, corresponding to ground, excited triplet, and singlet, respectively.

obtained from GW-BSE calculations. GW-BSE is the state of art to study excitons in materials<sup>17,52,53</sup> with excellent agreement with experiments. Our approach combines results from GW-BSE and Density Functional Perturbation Theory (DFPT)<sup>54-58</sup>. We call the negative of this gradient as Excited State Forces (ESF). In relaxation processes, we minimize the total energy, which is the sum of the ground state energy and the excitation energy  $E_T = E_{GS} + x\Omega$ , for a given exciton volumetric concentration  $x$ , until the total force  $F_T = F_{GS} - x\nabla\Omega$  is zero.

## II. OVERVIEW

The paper is organized in the following way: in section III we introduce the theory of ESF and the approximations used. In section IV we calculate ESF for the CO molecule and compare it with finite difference results. We also discuss the performance of approximations introduced in section III. On section V we analyze the ESF for LiF. We also relax its excited state and obtain a configuration where there is a self-trapped exciton with redshifted energy. Finally in section VIII we present our conclusions.

## III. THEORETICAL BACKGROUND

### A. Excited state forces - other approaches

Çaylak and Baumeier studied the relaxation of the excited state of small molecules<sup>40</sup> by performing GW/BSE calculations for different atomic configurations. Gradients of the excited state energies were obtained using finite differences, and in the case of large molecules with more degrees of freedom, just displacements that preserved the molecule symmetry were performed.

At TDDFT level, excited state forces can be calculated analytically<sup>59-65</sup>. They do not need approximations be-

yond the ones used in TDDFT (i.e. linear response) and depend on the quality of the exchange-correlation functional<sup>61</sup>. TDDFT works well in molecules, but standard DFT functionals do not reliably predict optical excitations in solids or nanostructures, because they lack the necessary long-range behavior to describe excitonic interactions<sup>66,67</sup>. So excited state forces calculated from GW-BSE results show the same advantages that GW-BSE calculations show in comparison to TDDFT.

In reference<sup>68</sup> a combination of constrained DFT (cDFT) and GW-BSE calculations is used. The excited states are relaxed at cDFT level, and once a configuration change path is obtained then exciton energies are calculated at GW-BSE level to refine the position of the minimum of the excited state energy surface. The cDFT relaxations do not include excitonic effects, just change the occupations in bands, although this approach may give good results if the studied exciton is well represented by the transition given by cDFT.

### B. Excited state forces - our approach

In 2003 Ismail-Beigi and Louie published an approach to calculate forces for the excited states in molecules and solids by combining solutions of the BSE and electron-phonon (ELPH) coefficients from Density Functional Perturbation Theory (DFPT)<sup>69</sup>. For the best of our knowledge, just one published work from the same authors used this approach in the last 20 years to study exciton self-trapping in SiO<sub>2</sub><sup>51</sup>. As GW/BSE calculations became more common in the materials science community<sup>52,53</sup>, we call attention to this method to study the relaxation of excited states. We revisit this theory and also analyze its convergence and performance in detail.

The basic concept in the excited state forces is that after absorbing light and creating an exciton  $|A\rangle$  with energy  $\Omega^A$  the total energy for a given system is given by  $E = E_0 + x\Omega^A$  where  $E_0$  is the ground state energy and  $x$  is the exciton volumetric concentration. For ground-state calculations, we are using Density Functional Theory using the Quantum Espresso package<sup>54-56</sup> and for the excited states we are using the BerkeleyGW code<sup>16,17,52,53</sup>. Computational details are provided in the supplemental material. This total energy depends parametrically on the atomic positions  $R$ , which defines a  $3N$  dimensional potential energy surface. The excited state force is given as the negative gradient with respect to the atomic positions of the exciton energy  $-\nabla\Omega^A$  and the total force is the sum of the excited state force times the exciton concentration  $x$  and the ground state force, which is well established in DFT codes. In reference<sup>70</sup> derivatives of the BSE hamiltonian with respect to the electric field were used to calculate dipole moments in a similar approach to the one used here.

For the derivative of the excitation energy, we use the Hellman-Feynman theorem:  $\nabla\Omega^A = \langle A|\nabla H^{\text{BSE}}|A\rangle$ , as  $\Omega^A$  and  $|A\rangle$  are eigenvalue and eigenvector of the BSE hamiltonian  $H^{\text{BSE}}$ , respectively. The BSE hamiltonian in the Tamm-Dancoff approximation is composed of two parts: an independent particle transition  $D_{cvk,c'v'k'} = (E_{ck}^{qp} - E_{vk}^{qp})\delta_{kk'}\delta_{cc'}\delta_{vv'}$ , where  $E_{ik}^{qp}$  is the quasi-particle energy of the state  $|ik\rangle$ , obtained in the

GW approximation<sup>16,52,53</sup>.  $D$  is diagonal in the basis of the transitions  $vk \rightarrow ck$  basis (represented by the ket  $|kcv\rangle$ ). The second part that composes the BSE hamiltonian is the kernel  $K^{\text{eh}}$  that contains the electron-hole interaction<sup>17,52,53</sup>. This kernel can be either a singlet or triplet kernel. Then the derivative of the excitation energy is given by  $\nabla\Omega^A = \langle A|\nabla D|A\rangle + \langle A|\nabla K^{\text{eh}}|A\rangle$

As it is observed in Ismail-Beigi and Louie's work<sup>69</sup> the derivatives of the kernel matrix elements can be neglected in comparison to the derivatives of the excitation energy. We also observe this fact and explore this approximation later in the text. Therefore we neglect the derivatives of the kernel matrix elements and use the following expression for the ESF

$$\begin{aligned} F_{i,\alpha}^S &= - \sum_{\nu} \langle A|\nabla_{\nu} H^{\text{BSE}}|A\rangle \hat{u}_{i,\alpha}^{\nu} \\ &= - \sum_{\nu k c v c' v'} A_{k c v}^* A_{k c' v'} (g_{c k, c' k}^{\nu} \delta_{v, v'} - g_{v k, v' k}^{\nu} \delta_{c, c'}) \hat{u}_{i,\alpha}^{\nu} \end{aligned} \quad (1)$$

, where  $i$  is one of the cartesian directions  $x, y, z$ ,  $\alpha$ , is an atomic index,  $\nu$  is the index of the displacement pattern  $\mathbf{u}^{\nu}$  (i.e. a phonon mode),  $g_{i k, j k}^{\nu}$  is the electron-phonon coefficient due to the collective atomic displacement  $\nu$  and  $A_{k c v} = \langle k c v|A\rangle$  is the exciton coefficient. One can identify equation 1 as the exciton-phonon coupling for excitons coupled to a zero-momentum phonon (or a linear combination of phonons)<sup>1,22-26,32,35,41</sup>, regardless of the exciton momentum.

Differently from reference<sup>69</sup> we consider the mixing of different conduction (valence) states by including off-diagonal electron-phonon coefficients, as the diagonal part of BSE hamiltonian becomes non-diagonal due to the atomic displacements  $D_{c v k, c' v' k'} = \langle c k|H^{\text{qp}}|c' k'\rangle - \langle v k|H^{\text{qp}}|v' k'\rangle$ . In reference to<sup>69</sup> two options for the ESFs are considered, one with (see equation 8 and one without (see equation 7) derivatives of kernel matrix elements. The second difference between our approach and the one used by Ismail-Beigi and Louie is the treatment of ELPH coefficients. ELPH coupling obtained from DFPT (DFT level) is underestimated in relation to ELPH calculated at GW level<sup>71-74</sup>. Frozen phonon calculations at GW level show that ELPH energies are normalized more than 40% for diamond<sup>71</sup>. Faber et. al<sup>73,74</sup> calculated the effective electron-phonon coupling potential  $V^{\text{ep}}$ <sup>88</sup> and observed that EPC effective potentials using self-consistent GW agreed better with experimental data than one shot  $G_0W_0$  and DFT results were substantially smaller than any GW calculation<sup>73</sup>. The same trends were observed for diamond and graphene in reference<sup>74</sup>. Li et al developed a self-consistent methodology to calculate el-ph coefficients at GW level, called GWPT, analogous to DFPT. This method had a better agreement to experimental data for the critical temperature for the superconductive phase of  $\text{Ba}_{1-x}\text{K}_x\text{BiO}_3$  than DFPT, with enhancements of ELPH coefficients up to 60%<sup>72</sup>. Splits of energy levels in diamond indicate an increase of about 15% in ELPH coefficients<sup>72</sup>.

The electron-phonon coefficients at GW level relate to the ones calculated at DFT level as

$$\langle i|\partial H^{\text{GW}}|j\rangle = \langle i|\partial H^{\text{DFT}}|j\rangle + \langle i|\partial(\Sigma - V_{xc})|j\rangle \quad (2)$$

, where  $\Sigma$  is the self-energy operator and  $V_{xc}$  is the exchange-correlation functional<sup>16</sup>. This task can be done either using FD or GWPT<sup>72</sup>, although both options are highly computationally demanding in comparison to DFPT. In references<sup>22,32,69,70</sup>, electron-phonon coefficients are calculated directly from DFPT calculations, neglecting the derivatives of  $(\Sigma - V_{xc})$ . We chose to use a renormalization scheme that is based on the approximation that the eigenvectors from the DFT hamiltonian are the same eigenvectors of the quasiparticle hamiltonian, which is the essence of the one-shot GW approximation<sup>16</sup>. This scheme is given by<sup>75,76</sup>

$$\langle i|\partial H^{\text{qp}}|j\rangle = \begin{cases} \left( \frac{E_i^{\text{qp}} - E_j^{\text{qp}}}{E_i^{\text{dft}} - E_j^{\text{dft}}} \right) \langle i|\partial H^{\text{dft}}|j\rangle, & \text{if } E_i^{\text{dft}} \neq E_j^{\text{dft}} \\ \langle i|\partial H^{\text{dft}}|j\rangle, & \text{else.} \end{cases} \quad (3)$$

The diagonal matrix elements remain the same while off-diagonal matrix elements are renormalized based on QP and DFT energy level differences. We explore the performance of this approximation in sections IV A and IV B.

### C. Code implementation

One practical problem that Ismail-Beigi and Louie faced, is that in calculations for the CO molecule including derivatives of the kernel, the ESF on the C and O atom did not obey Newton's third law, where the forces on the molecule center of mass was about  $2 \text{ eV}/\text{\AA}$ <sup>69</sup>. One solution to this issue was to subtract the force on the center of mass after the ESF calculation. They attributed this fact to the approximation  $\delta W/\delta G \approx 0$  ( $W$  is the screened coulomb interaction and  $G$  the Green's function used in the GW approximation). We noticed that actually this issue is caused intrinsically by the not obedience of the acoustic sum rule by the ELPH coefficients from DFPT calculations in Quantum Espresso code. Therefore the approximation  $\delta W/\delta G \approx 0$  can still be safely used. We solved this problem by applying an Acoustic Sum Rule (ASR) to the ELPH coefficients. Both our method, where we neglect derivatives of the kernel, and Ismail-Beigi and Louie's method including derivatives of the kernel, presented results where the ESF on the center of mass is zero after we applied this ASR on the ELPH coefficients. In the supplemental material, we discuss how we apply the ASR.

In reference<sup>69</sup> ESF neglecting kernel derivatives differed from FD calculations by about  $4 \text{ eV}/\text{\AA}$ , while with the inclusion of kernel derivatives, ESF had a better agreement with FD but in tests for the CO molecule the forces on carbon and oxygen atoms differed by about  $2 \text{ eV}/\text{\AA}$

The wavefunctions that are used to calculate the ELPH coefficients must be the same used to create the BSE hamiltonian, so the coefficients  $A_{k c v}$  and  $g_{i k, j k}^{\mu}$  are consistent regarding their complex phases<sup>37</sup>. In the BerkeleyGW code<sup>52</sup> in general, one computes the quasiparticle energies (GW approximation) and kernel matrix elements  $\langle c v k|K|c' v' k'\rangle$  in a coarse grid and then interpolates those quantities to a fine grid where the BSE hamiltonian is built. We work with two possibilities:

1. the DFPT coefficients are calculated in the fine grid and 2. the DPFT are calculated in the coarse grid and one can use interpolation coefficients used by the BerkeleyGW code to compute the DFPT coefficients in the fine grid. Other schemes can also be used as Wannier interpolation<sup>77–79</sup>.

#### IV. EXCITED STATE FORCES VS FINITE DIFFERENCES IN CO

We start by analyzing excited state forces using equation 1 for the singlet ( $A^1\Pi$ ) and triplet ( $A^3\Pi$ ) excitons in the CO molecule and our results are summarized in Figure 2. As the CO molecule has one degree of freedom, we can easily compare results that used analytical ESF with finite differences (FD). First, we note that the FD curves are not as smooth as the curves using our method and the methods in reference<sup>69</sup>. This is due to the limited size of the BSE hamiltonian and as we change the bond length the nature of the conduction states included in BSE changes. We also show results obtained from centered two-point finite difference using the exciton energies. We note that our method agrees very well with the method from<sup>69</sup> either with we use the normalized ELPH coefficients or not (the curves are on top of each other). This is more evident in the bar plots on the right side of figure 2. The renormalization of ELPH coefficients makes our calculations agree better with finite difference results in the region  $R_{CO} < 1.1 \text{ \AA}$ , while in the region  $R_{CO} > 1.1 \text{ \AA}$  it does not influence substantially. In the triplet case, the discrepancy among all methods becomes smaller.

In table I we compare the equilibrium distance (where the excited state force has the same magnitude and opposite direction to the DFT force) of the CO bond for the singlet and triplet excitons with experimental data and other ab initio studies. Our results deviate from experimental values by a few pm.

We notice that the ESF for the CO is repulsive for both singlet and triplet excitons. Those excitons are composed by conduction states with antibonding character and valence state with bonding character. As the CO bond length increases the split between those the two energy levels of the states that compose this exciton decreases, therefore the ESF will be repulsive. In the appendix, we show that a simple tight-binding model provides physical insight into why the ESF is repulsive in this case.

The great agreement between our method and the method from reference<sup>69</sup> when the kernel derivative is included is due to the fact that the derivative of the kernel term  $\partial(A|K|A)$  is equal to the off-diagonal matrix elements that we included in equation 1. A derivation of those equations is provided in section XXXX.

##### A. Diagonal matrix elements ELPH coefficients

Now we go deeper in the approximations used in our approach.

We first analyze the diagonal matrix elements. Using the Hellman-Feynman theorem, the derivatives of the DFT energy levels are equal to the diagonal ELPH

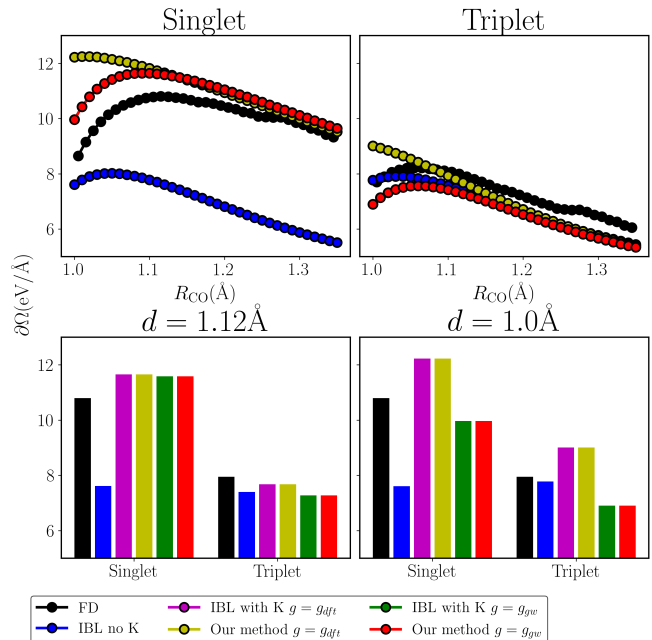


**Figure 2:** Derivative of excitation energy for the first exciton in CO for singlet (a) and triplet (b) using our method and method from<sup>69</sup> with and without derivatives of kernel. When derivatives of off-diagonal electron-phonon matrix elements are present we perform calculations with and without renormalization using equation 3. Subpanels (c) and (d) show the derivatives of  $\Omega$  when the bondlength is 1.0 and 1.12  $\text{\AA}$  respectively. Our method agrees with method from<sup>69</sup> with derivatives of kernel regardless of the renormalization of elph coefficients.

matrix elements  $\partial E_n^{dft} = \langle n | \partial H^{dft} | n \rangle$ . A common approximation used in GW calculations is that the QP and DFT hamiltonians share the same eigenvectors (the  $\Sigma - V_{xc}$  operator is diagonal in the basis of the DFT eigenvectors), so in this case one can also write  $\partial E_n^{qp} = \langle n | \partial H^{qp} | n \rangle$ , then the difference between both derivatives is  $\partial E_n^{qp} - \partial E_n^{dft} = \langle n | \partial(\Sigma - V_{xc}) | n \rangle$ . We neglect this difference and approximate  $\partial E_n^{qp} \approx \partial E_n^{dft} =$ . This is the same as it was done in reference<sup>69</sup>. Further work is necessary to deal with the term  $\langle n | \partial(\Sigma - V_{xc}) | n \rangle$ .

To analyze the quality of this approximation we show in figure 3 the variation of the QP energy levels vs the variation of DFT energy levels when we change the CO bondlength from 1.1 to 1.35  $\text{\AA}$ . We can see here that those two variations are correlated to each other and are, approximately, over the  $y = x$  curve.

##### B. Off-diagonal ELPH matrix elements

Now we look at the off-diagonal matrix elements derivatives. In this case, we approximate the term  $\langle n | \partial(\Sigma - V_{xc}) | m \rangle$  to be  $(E_n^{qp} - E_m^{qp}) / (E_n^{dft} - E_m^{dft}) - 1$ , which leads to the first line of the equation 3. We compare this renormalization with scheme on DFPT ELPH coefficients with crude DFPT coefficients to reproduce FD calculations. The finite differences calculations were performed using the following equation

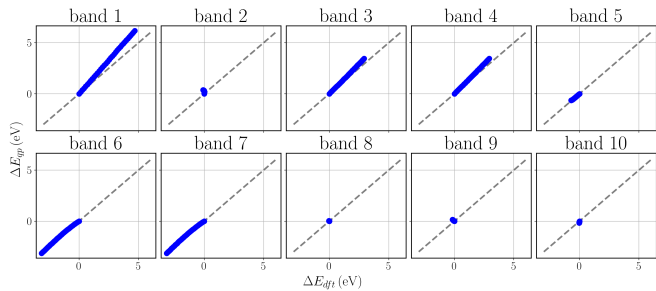


**Figure 3:** QP energy variations vs DFT energy variations. Those energies were calculated from changing the  $R_{CO}$  bond length from 1.1 to 1.35 Å to bands 1 to 10 in CO molecule. The first five bands are full occupied. Vertical  $y = 0$ , horizontal  $x = 0$  and diagonal  $y = x$  dashed black lines are guides to the eye.

$$\begin{aligned} \langle i | \partial H^{qp} | j \rangle_{\text{FD}}(R) &= \langle i | \partial H^{\text{dft}} | j \rangle_{\text{DFPT}}(R) \\ &+ \frac{\langle i_R | (\Sigma - V_{xc})_{R+\delta R} - (\Sigma - V_{xc})_{R-\delta R} | j_R \rangle}{2\delta R} \end{aligned} \quad (4)$$

where  $\langle i | \partial H^{\text{dft}} | j \rangle_{\text{DFPT}}(R)$  is the ELPH coefficient calculated at DFT level using DFPT, and the second term is calculated using FD. The  $(\Sigma - V_{xc})$  operator is constructed with wavefunctions of CO with bond lengths  $R \pm \delta R$  ( $\delta R = 10^{-4}$  Å), and this operator is evaluated in the basis  $|i_R\rangle$ , the state  $i$  calculated for a CO bond length equal to  $R$ . Our results are summarized in Figure 4. In fact, we observe a mean increase for ELPH coefficients by about 35% using our method in relation to ELPH from DFPT. By looking at Figure 2, we see that our excited state forces perform better when we use our renormalization scheme.

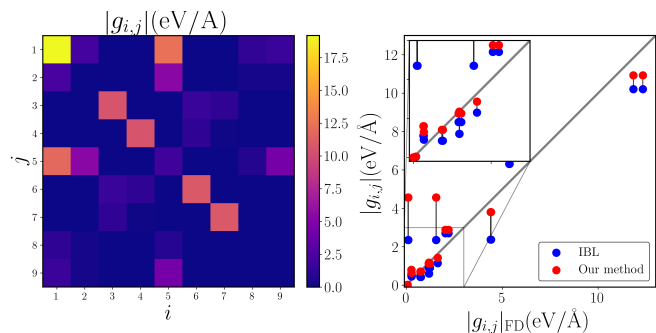


**Figure 4:** Left: elph coefficients calculated at FD differences (see text). Right: elph coefficients calculated using our renormalization scheme (red dots) and from DFPT data (blue dots) that is the approximation used in<sup>69</sup> as function of the elph coefficients calculated using FD. The closer the data is from the black dashed line  $y = x$  the better is the agreement of the method with FD calculations.

### C. Kernel derivatives

Derivatives of kernel can be neglected as their variations is relatively small compared to the RPA part of BSE hamiltonian<sup>22,69</sup>. We also verified in figure 5 that the variations of the kernel are substantially smaller than the variation of the expectation value of kernel for the

first ten exciton in CO with bond length equal to 1.12 Å. In figure 21 (Supplemental material) we explore the variation of the kernel energy by changing the bond length from 1.1 to 1.35 Å and we observe the same trend.

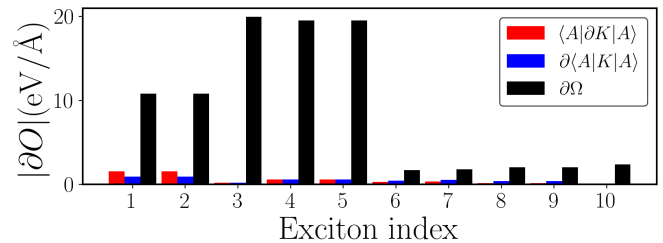


**Figure 5:** Derivative of kernel for the ten first excitons in CO with bond length equal to 1.12 Å. In red just the operator changes, while in blue the states are allowed to change as well. In black we show the derivatives of the excitation energy. We can see that the derivatives of the kernel represent just a small fraction of the excitation energy derivative.

In reference<sup>80</sup> van der Walls excited state forces are studied with the approximation that the exchange kernel is more important in long-range distances, as the direct kernel depends on the orbital overlap.

### D. Convergence of excited state forces calculations

In BSE calculations one chooses how many conduction and valence bands will be included in the BSE Hamiltonian. This choice is made to include sufficient bands to converge the exciton energies of interest and absorption spectra. In the specific case of molecules the necessary number of conduction bands to be included is of the order of a few hundreds<sup>81</sup>. Here we observe that the convergence of excited state forces follows the same tendency as the convergence of the exciton energy. As an example, we show in Figure 6 the convergence of the energy, excited state forces, and most important  $A$  coefficients for the lowest singlet exciton in CO with bond length equal to 1.12 Å. For this exciton the most important transitions are  $v_1 \rightarrow c_1$  and  $v_1 \rightarrow c_2$  ( $c_1$  and  $c_2$  here are degenerate). As the excited state forces and excitation energies depend on the  $A_{kcv}$  coefficients, then we observe that those three quantities follow the same trend with respect to the number of conduction bands in the BSE. In Figure 6.d we show that the variation of the excitation energy and the variation of the excited state force from our most converged results follow a linear relation with each other.

## V. EXCITED STATE FORCES IN LIF

Now we move to the analysis of ESF on LiF. We start computing ESF for its rocksalt structure with  $O_h$  point group symmetry. We observe that the excited state forces are essentially zero due to the system symmetry.

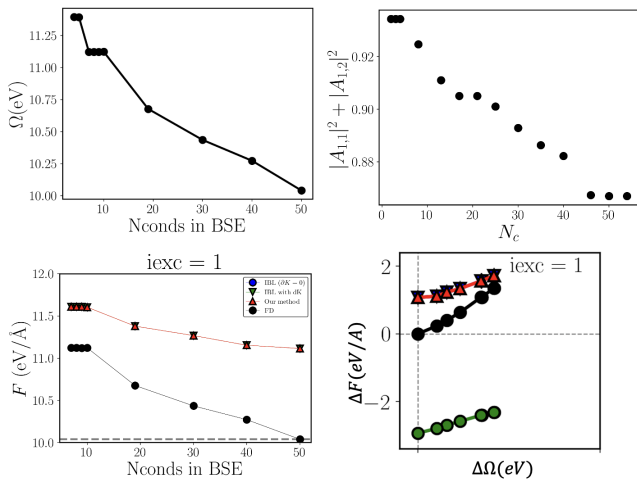


**Figure 6:** Convergence of excitation energy, excited state forces and most important coefficients for the first exciton in CO.

### A. Random displacements investigations

One can apply displacements to break the system symmetry to relax the excited state. Those displacements can be random or based on physical intuition about a particular case. For our demonstration, we applied random displacements using gaussian distribution with a standard deviation temperature dependent equal to  $\sigma_i = \sqrt{k_b T / \lambda_i}$ , where  $\lambda_i$  is the eigenvalue  $i$  of the force constant matrix  $K$ .

### B. Relaxation of excited state structures

Once the random displacement is applied then we relax the system using Newton's method. Other methods as steepest descent and conjugate gradient are also perfectly good options. For each relaxation step, we calculate the analytical excited state force and force constant matrix from DFPT. The total displacement is given by

$$\delta r = \sum_i \hat{u}_i \min((\vec{F} \cdot \hat{u}_i) / \lambda_i, \text{limit}) \quad (5)$$

where  $\lambda_i$  and  $u_i$  are the  $i$ -th eigenvalue and the  $i$ -th eigenvector of  $K$ .

The results for our relaxation are shown in figure 7. We observe that the total energy decreases until convergence. We also monitor the total force that reaches zero.

This shows how our analytical ESF can be used to study self-trapped excitons in materials. This study for LiF corresponds to 1 exciton per one unit cell ( $6 \times 10^{22}$  excitons /  $\text{cm}^3$ ), which is an extreme exciton concentration. The exciton trapping energy is about 150 meV and the redshift in the absorption spectra is 0.4 eV. The relaxed structure belongs to  $C_{3v}$  point group while the rocksalt LiF belongs to  $O_h$ . We observe the valence band at the  $\Gamma$  point, originally triple degenerate, splits in one double degenerate and one single band and there is a decrease of the main gap at the  $\Gamma$  point. This leads to the splitting of the first absorption peak, creating one redshifted and one blueshifted peak.

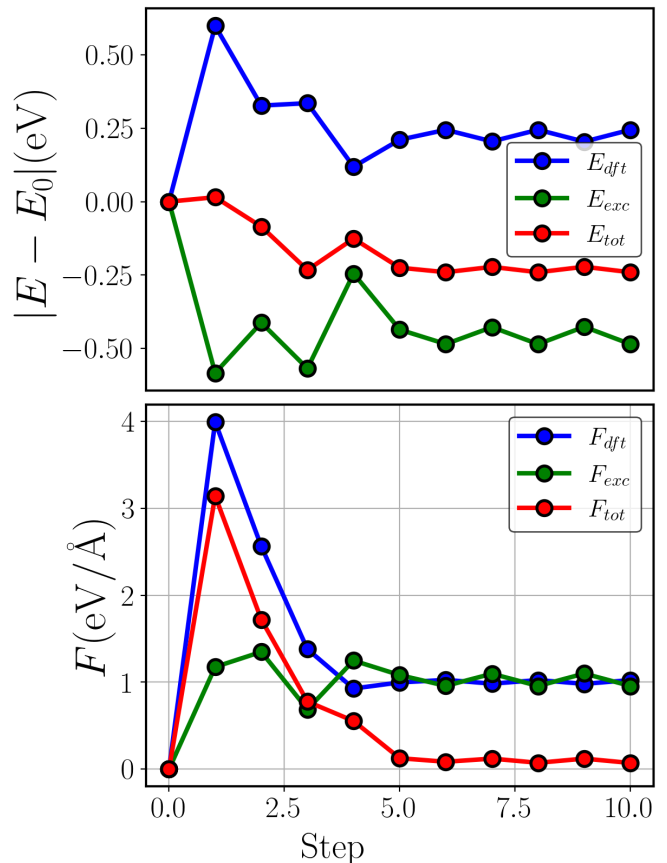


**Figure 7:** Energies variations (upper panel) and forces (lower panel) on LiF during relaxation of the ESF summed to the DFT force. Step zero corresponds to the RS structure, for which both the ESF and DFT forces are null due to symmetry. Step one corresponds to random displacement and step ten corresponds to the STE configuration.

### C. Symmetry-based path of trapping excitons

As the relaxed excited state configuration has  $C_{3v}$  symmetry we now investigate the transition from rocksalt to this relaxed structure. To do this we move the fluoride atom in the direction where the  $C_{3v}$  symmetry is preserved (see Fig. 8). We see that initially the DFT increases and the first exciton energy decreases, while the total energy has a minimum at  $\delta r \approx 0.6 \text{ \AA}$ . We observe a small energy barrier of 13 meV.

In Figure 9 we show the evolution of the LiF absorption spectra as we move the fluorine atom. The peak initially at 12.1 eV and composed by three excitons, splits in two new peaks. One peak is composed by two excitons and is blueshifted while other is composed by one exciton is initially redshifted and then after  $\delta r \approx 0.6 \text{ \AA}$  this peak is blueshifted. We also show the evolution of the energies of the three first excitons.

The split of the triply degenerate exciton is explained by its bandstructure. At the  $\Gamma$  point the valence band is triply degenerate and has  $p$  orbital character, while the conduction band is non-degenerate. As we move the fluoride atom this triply valence band breaks in one doubly degenerate and one non-degenerate. In Figure 10 we show the split of the valence band. This leads to two gaps close in energy, and one gap increases and the other decreases as we move the fluoride atom.

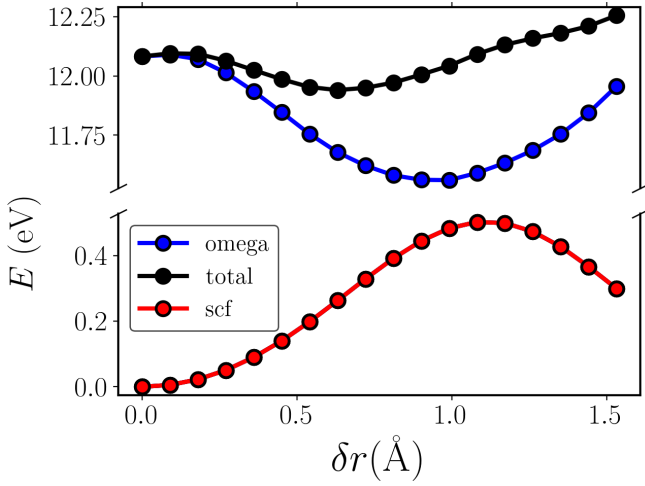


**Figure 8:** DFT, excitation and total energies for the first exciton as function of the displacement of the F atom through LiF unit cell. The  $C_{3v}$  symmetry is preserved during this displacement.

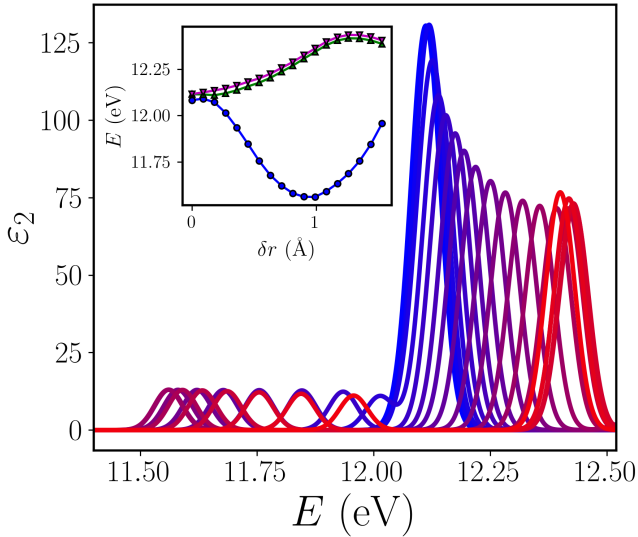


**Figure 9:** Evolution of the absorption spectra of LiF. The main peak at 12.1 eV splits in one blueshifted and one redshifted peaks. The energies of the first three excitons are also shown in the inset of the figure.

Along this path, both the excited state force and the DFT force are parallel to the atomic displacement as shown in figure 11. We obtain a good agreement between analytical ESF and FD ESF, which shows the efficiency of our method.

#### D. Derivatives of diagonal elph matrix elements - STE

We now analyze the performance of our approximations on ELPH coefficients and kernel derivatives for LiF in the STE configuration, as in the rocksalt configuration diagonal ELPH coefficients and kernel derivatives are null due to symmetry.

First, we look at the diagonal ELPH coefficients. We observe that in general the approximation  $\partial E_{ik}^{qp} \approx \partial E_{ik}^{dft}$  can be used as the DFT derivatives underestimate QP derivatives about 30% for the eight first bands in LiF

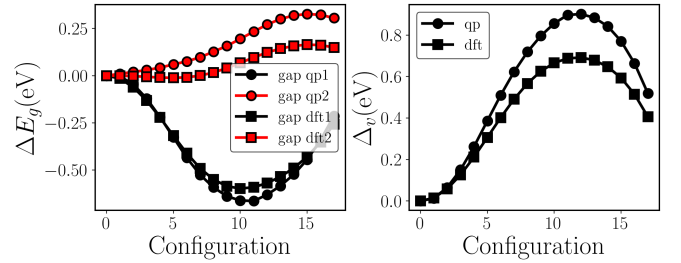


**Figure 10:** Left: First and second gaps at the  $\Gamma$  point for LiF as function of displacement of F atom. Right: split of the valence band.

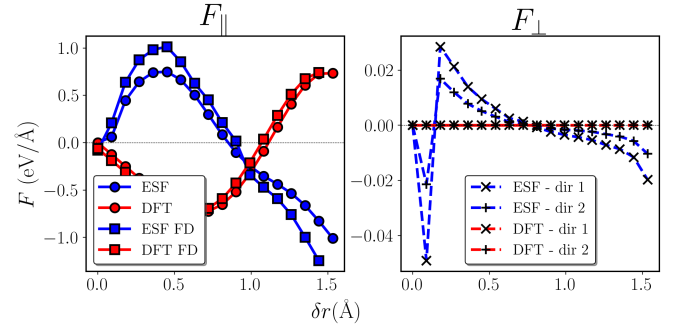


**Figure 11:** ESF and DFT forces on the F atom as function of its displacement. On the left we show the forces components parallel to the atomic displacements, while in the right we show components perpendicular. The parallel component is much larger than the perpendicular components.

and all 64 k points that we analyzed as shown in figure 13.

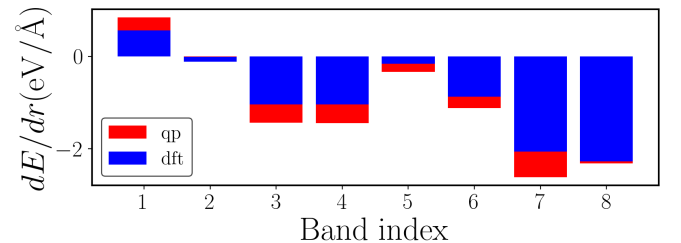


**Figure 12:** Derivative of DFT (blue bars) and QP (red bars) energy levels for the first eight bands in LiF at the  $\Gamma$  point. The first five bands are valence bands.

#### E. Derivatives of offdiagonal elph matrix elements - STE

Then we analyze the offdiagonal ELPH matrix elements. In this case both DFT and our approximation (equation 3) underestimate ELPH coefficients at QP level obtained by FD as shown in Figure14. Looking at the mean deviation of those results with respect to FD calculations, both our renormalization scheme and DFT data underestimate ELPH coefficients by about 0.5 to 1.5 eV/Å, although our renormalization show a slightly better performance.

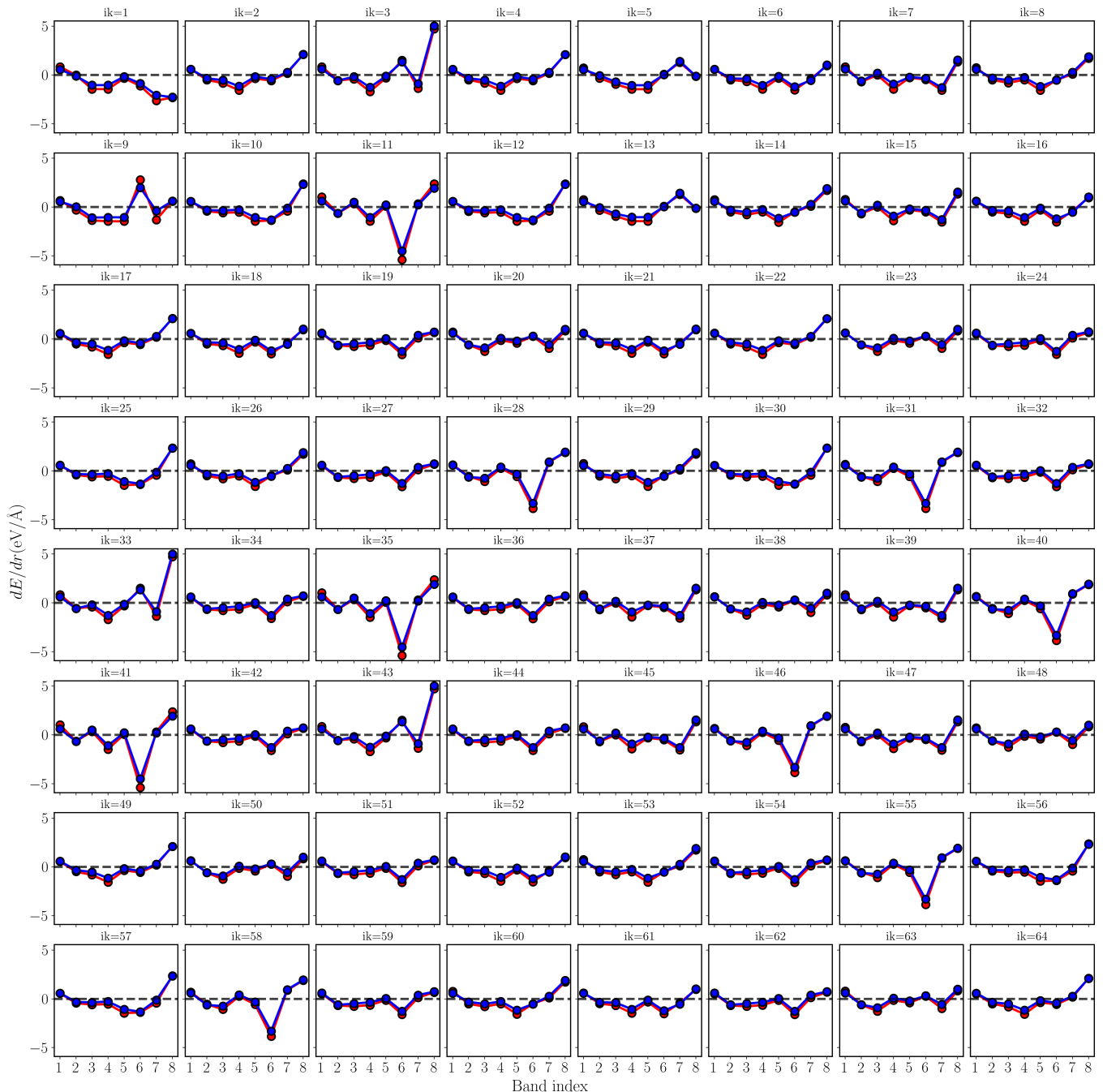


**Figure 13:** Derivative of DFT (blue points) and QP (red points) energy levels for the first eight bands in LiF. The first five bands are valence bands. Each subplot is for a different  $k$  point in a  $4 \times 4 \times 4$   $k$  grid.

## F. Changes in Kernel - STE

Now we look at the derivatives of kernel. On figure 16 we observe that in general derivatives of kernel are a fraction of the derivatives of the ESF, although in cases where  $\partial\Omega$  is smaller than  $0.25$  eV/Å the derivatives of the kernel are of the same order as the derivatives of the excitation energy.

## VI. RELAXATION SCHEMES

### VII. ESF AND SOC

Now we discuss the ESF when including Spin Orbit Coupling (SOC). In the case of semiconductors where the SOC splittings are much smaller than the material bandgap, one can include the SOC interactions perturbatively as it is done in the references<sup>82</sup>. In this approximation the excitation energy is given by  $\Omega_\sigma^A = \Omega^A + \Delta\Omega_\sigma^A$ , where the second term is the perturbation correction given by  $\Delta\Omega_\sigma^A = \sum_{cvk} |A_{cvk}|^2 [(E_{ck}^{qp} + \Delta E_{ck\sigma}^{qp}) - (E_{vk}^{qp} + \Delta E_{vk\sigma}^{qp})]$ , where  $\Delta E_{ik\sigma}^{qp}$  is the variation of GW calculations including SOC effects in relation to GW calculation without SOC effects. With this approximation, the excited state forces



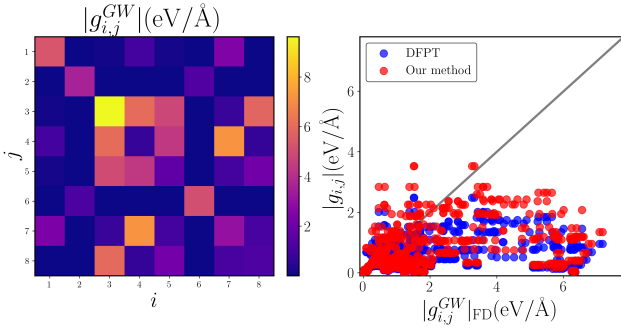


**Figure 14:** ELPH coefficients for LiF. Left: ELPH coefficients at GW level calculated by finite differences (see equation 4). Right: comparison of ELPH calculated at DFPT level and using our renormalization scheme 3.

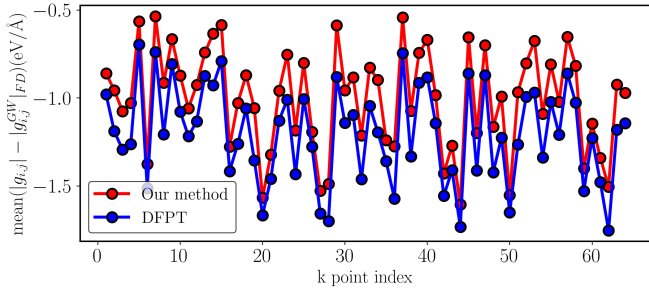


**Figure 15:** Mean deviation of ELPH coefficients from DFPT and our method with respect to ELPH coefficients calculated at FD. The mean is take over different bands.

have a correction given by

$$\Delta F = -\nabla \Delta \Omega_{\sigma}^A = -\sum_{cvk} |A_{cvk}|^2 (\nabla \Delta E_{ck\sigma}^{qp} - \nabla \Delta E_{vk\sigma}^{qp}) \quad (6)$$

In the above equation, the gradient  $\nabla \Delta E_{ik\sigma}^{qp}$  is equal to the difference of diagonal ELPH coefficients calculated with and without SOC interactions. To understand the importance of this term we analyze the difference between those two terms for the  $A_1'$  phonon mode in MoS<sub>2</sub> monolayer, where the two sulfur atoms move perpendicular to the monolayer plane in opposite directions and the molybdenum atom remains stopped. We observe in figure 18 that this difference is negligible in comparison to the magnitude of the diagonal ELPH coefficients, therefore the ESF theory can be safely applied in systems where SOC can be treated with perturbation theory.

## VIII. CONCLUSIONS

We have presented a practical workflow to calculate ESF from GW-BSE calculations that combines excitonic effects with electron-phonon effects. This approach is based on the reference<sup>69</sup>, where we solved the non-zero force on the system center of mass issue and studied extensively the quality and validity of approximations used in our approach. Then the ESF can be used in optimizing algorithms in order to relax excited states. We also have studied the self-trapping mechanism of excitons in a primitive cell of LiF, and in this case we observed a split of the first absorption peak with a redshifted signal. In the reference [Our other paper](#) we study the self-trapping

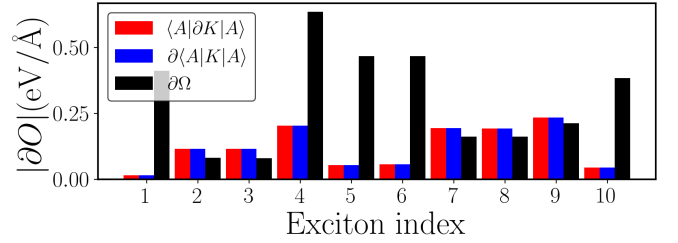


**Figure 16:** Derivatives of kernel compared to derivatives of the excitation energy for LiF.

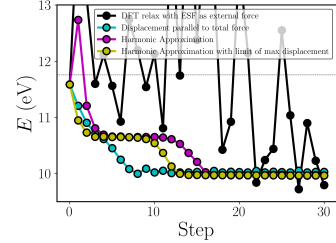


**Figure 17:** Caption

mechanism for  $V_k$  center in LiF, while on reference [BGW paper](#) we relate the ESF with the generation of coherent phonons in monolayer MoS<sub>2</sub>. Therefore the ESF theory can be applied to the microscopic mechanisms of the interaction of light with matter.

## Acknowledgments

D.A.S. was supported by the U.S. Department of Energy, Office of Science, Basic Energy Sciences, CTC and CPIMS Programs, under Award DE-SC0019053. R.R.D.G. and D.A.S. were supported by the U.S. National Science Foundation under Grant No. DMR-2144317 and Cottrell Scholar award No. 26921, a program of Research Corporation for Science Advancement; and this material is based upon work supported by the Air Force Office of Scientific Research under

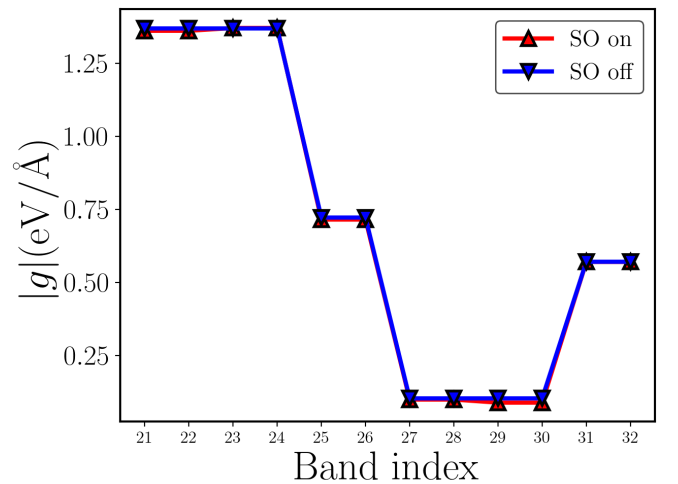


**Figure 18:** Diagonal electron-phonon coefficients for monolayer MoS<sub>2</sub> with and without SOC. The mode shown here is the  $A_1'$ , where the two sulfur atoms move towards each other and the molybdenum atom does not move.

award number FA9550-19-1-0236. Computational resources were provided by the National Energy Research Scientific Computing Center (NERSC), a U.S. Department of Energy Office of Science User Facility operated under Contract No. DE-AC02-05CH11231; the Texas Advanced Computing Center (TACC) at The University of Texas at Austin (<http://www.tacc.utexas.edu>); and the Pinnacles and Multi-Environment Computer for Exploration and Discovery (MERCED) clusters at UC Merced, funded by National Science Foundation Grants No. OAC-2019144 and ACI-1429783.

## IX. APPENDIX

### A. Equations used - ESF

In Ismail-Beigi and Louie's work<sup>69</sup> two expressions for ESF can be found. The first one is

$$\partial\Omega = \sum_{kcv} |A_{kcv}|^2 (g_{ck,ck}^\mu - g_{vk,vk}^\mu) \quad (7)$$

where  $g_{ik,jk'}^\mu = \langle ik | \partial H^{df} | jk' \rangle$ . This expression neglects the kernel matrix elements derivatives. The expression that includes kernel derivatives is

$$\partial\Omega = \sum_{kcv} |A_{kcv}|^2 (g_{ck,ck}^\mu - g_{vk,vk}^\mu) + \partial K_{kcv,k'c'v'} \quad (8)$$

where  $\partial K_{kcv,k'c'v'}$  are derivatives of kernel matrix elements and are given by

$$\begin{aligned} \partial K_{kcv,k'c'v'} = & \langle \partial(kc)vk | K | k'c'v'k' \rangle + \\ & \langle kc\partial(vk) | K | k'c'v'k' \rangle + \\ & \langle kcvk | K | \partial(k'c')v'k' \rangle + \\ & \langle kcvk | K | k'c' \partial(v'k') \rangle \end{aligned} \quad (9)$$

and the derivatives  $|\partial ik\rangle$  are expanded using first-order perturbation theory using a perturbation of the DFT hamiltonian. The term  $\langle kcv | \partial K | k'c'v' \rangle$  is neglected. The conduction state derivatives are given by

$$|\partial ck\rangle = \sum_{c'k} \frac{\langle c'k | \partial H^{df} | ck \rangle}{(E_{c'k}^{df} - E_{ck}^{df})} |c'k\rangle. \quad (10)$$

and a similar expressio for valence states. The above equation assumes no mixing of conduction and valence states. This assumption is valid for semiconductors with a sufficient large bandgap, where the Tamm-Dancoff approximation is valid<sup>17</sup>.

### B. Renormalization of ELPH coefficients

We start from the definition of the QP hamiltonian matrix elements

$$H_{ij}^{qp} = H_{ij}^{df} \delta_{ij} + \Delta \Sigma_{ij} \delta_{ij} \quad (11)$$

where  $|i\rangle$  is an eigenstate of the DFT hamiltonian with eigenvalue  $E_i^{df}$  and  $\Delta \Sigma_{ij} = \langle i | \Sigma - V_{xc} | j \rangle$ . The state  $|i\rangle$  is also eigenstate of the QP hamiltonian. Using, first order perturbation theory we have that

$$|\partial i\rangle = \sum_{k \neq i} \frac{\langle k | \partial H^{df} | i \rangle}{E_i^{df} - E_k^{df}} |k\rangle \quad (12)$$

But as this state is also an eigenstate of the QP hamiltonian, we can write

$$|\partial i\rangle = \sum_{k \neq i} \frac{\langle k | \partial H^{qp} | i \rangle}{E_i^{qp} - E_k^{qp}} |k\rangle \quad (13)$$

This implies that

$$\frac{\langle j | \partial H^{df} | i \rangle}{E_i^{df} - E_j^{df}} = \frac{\langle j | \partial H^{qp} | i \rangle}{E_i^{qp} - E_j^{qp}} \quad (14)$$

which leads to equation 3.

### C. Acoustic Sum Rule on ELPH coefficients

In reference<sup>69</sup> the excited state forces using the kernel on the C and O atoms are different from each other. They attributed this to their approximation  $\partial W \approx 0$ . We also faced this problem when using equation 1. In our investigations, we calculated the sum of electron-phonon coupling coefficients given by

$$S_{ij}^n = \sum_{\nu} \langle i | \partial_{\nu} H^{df} | j \rangle (\hat{n} \cdot \hat{\nu}) \quad (15)$$

where  $\hat{\nu}$  is the  $3N$  component unitary vector parallel to the phonon mode displacement and  $\hat{n}$  is the  $3N$  component vector that represents the system center of mass displacement in the  $x$ ,  $y$  or  $z$  directions. This quantity should be zero, as a pure center of mass displacement should have  $\partial V_{scf} = 0$ . We noticed that it was not obeyed in the case of the CO molecule, even when performing those test calculations with different pseudopotentials. We also checked that this was not a convergence issue as shown in figure 19. Our solution to this was to apply an Acoustic Sum Rule (ASR) to impose the sum in equation 15 to be zero. We verified that this has the same effect as imposing that the force on the center of mass is zero, as it is done in reference<sup>69</sup>.

### D. Computational Details

For all calculations, we used scalar relativistic LDA pseudo potentials from pseudo-dojo website<sup>83</sup>. All GW calculations were performed with Generalized Plasmon Pole approximation for frequency dependency of the self-energy<sup>16</sup> and the static remainder coulomb-hole<sup>84</sup>. For CO DFT calculations the kinetic energy cutoff is equal to 100 Ry and the k-grid was composed just by the  $\Gamma$  point. In GW calculations the dielectric matrix was built with 500 empty states and a cutoff of 20 Ry for the screened Coulomb interaction. The BSE hamiltonian was built

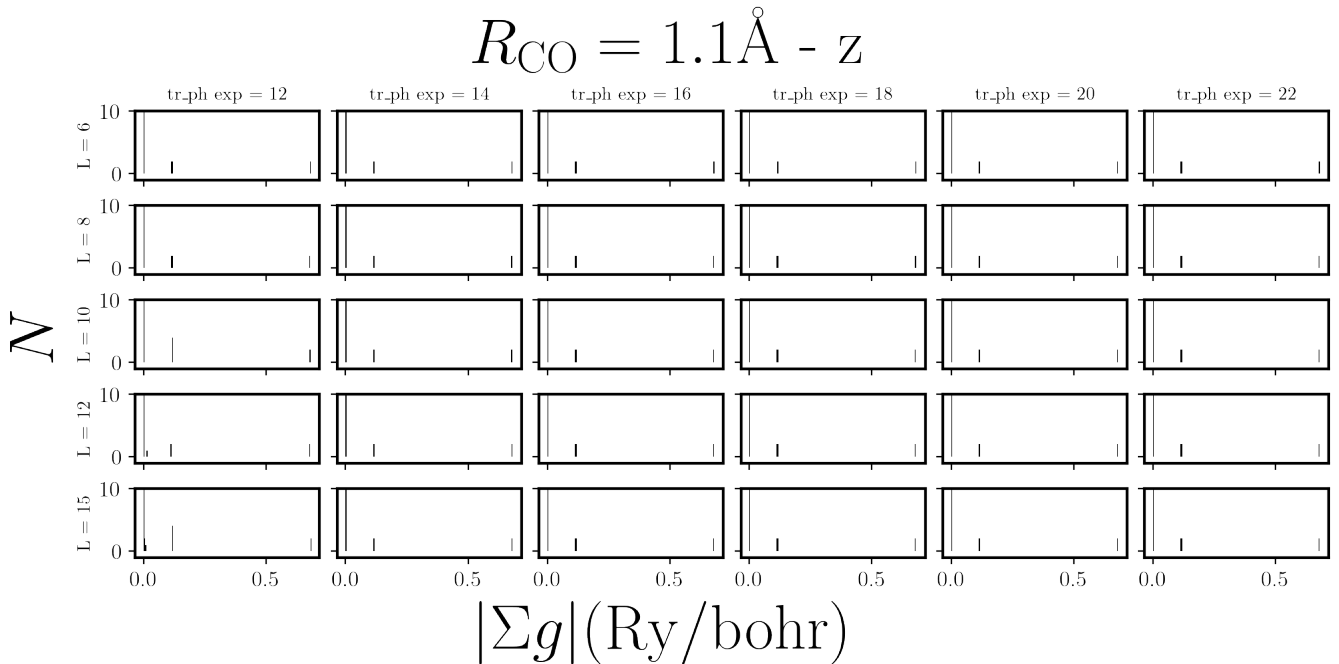


**Figure 19:** Histograms of sums of ELPH coefficients due to displacement of the C and O atom in the  $\hat{z}$  direction (parallel to the CO bond). ELPH coefficients due to movements perpendicular to  $\hat{z}$  are negligible. As those displacements are in the same direction, their sum should be zero. Each sum is given by equation 15. We performed this analysis by varying the cubic supercell size from 6 to 15Å and varying the DFPT threshold from  $10^{-12}$  to  $10^{-22}$ .

with 5 valence states and 13 conduction states. For LiF DFT calculations the kinetic energy cutoff is equal to 80 Ry and the k-grid was a regular k-grid  $4 \times 4 \times 4$  centered at the  $\Gamma$  point. The relaxed lattice parameter was 2.02948 Å. For GW/BSE calculations we used a coarse grid of  $4 \times 4 \times 4$  and a fine grid of  $8 \times 8 \times 8$ , both centered at  $\Gamma$ . In GW calculations the dielectric matrix was built with 300 empty states and a cutoff of 20 Ry for the screened Coulomb interaction. The BSE hamiltonian was built with 5 valence states and 10 conduction states.

### E. Practical workflow

Now we present a practical workflow for excited state forces calculations. Here we present how it should be used for semiconductors.

The GW/BSE calculations in BerkeleyGW code consist basically of four steps

1. Epsilon - calculation of the dielectric matrix using wavefunctions with a high number of conduction bands.
2. Sigma - calculation of quasiparticle energy levels on a coarse grid.
3. Kernel - calculation of the kernel that contains the electron-hole interaction on a coarse grid.
4. Absorption - interpolation of kernel and quasiparticle energy levels from a coarse to a fine grid, constructs and solves the BSE hamiltonian, and then calculates the optical absorption.

where those quantities are calculated from results of DFT calculations.

Our code reads the interpolated quasiparticle energy levels and exciton wavefunctions from the BerkeleyGW absorption step. Then, we calculate the electron-phonon coefficients using the same wavefunctions used in the fine grid step. Examples of calculations are provided in the webpage [XXX](#).

### F. Tight binding model for ESF

To understand the physics of the excited state forces, we will analyze the  $\text{H}_2^+$  molecule. In a tight binding model, the HOMO and LUMO energy levels are given by<sup>85</sup>

$$E_{\text{HOMO(LUMO)}} = E_{1s} + \frac{j_0}{R} + \frac{j \pm k}{1 \mp S} \quad (16)$$

where  $j_0 = e^2/4\pi\epsilon_0$  ( $e$  is the electron charge and  $\epsilon_0$  the vacuum dielectric constant),  $E_{1s} = 13.6$  eV,  $R$  is the distance between the hydrogen atoms,  $a_0$  is the Bohr radius, the other quantities are given by

$$j = \frac{j_0}{R} \left( 1 - \left( 1 + \frac{R}{a_0} \right) e^{-2R/a_0} \right) \quad (17)$$

$$k = \frac{j_0}{a_0} \left( 1 + \frac{R}{a_0} \right) e^{-R/a_0} \quad (18)$$

and the overlap  $S$  is given by

$$S = \left( 1 + \frac{R}{a_0} + \frac{1}{3} \frac{R^2}{a_0^2} \right) e^{-R/a_0} \quad (19)$$

The bandgap is given by

$$E_g = \frac{2(k - Sj)}{1 - S^2} \quad (20)$$

An exciton composed of the HOMO and LUMO states has energy equal to  $\Omega = E_g + K$ . In this case, we approximate the kernel derivative to be zero, which is a common approximation we use in the main text. An analytical expression for the derivative of the gap is quite complicated. We can analyze the plot of  $E_g$  as a function of the nucleus distance. We observe that the gap decreases when  $R$  increases, as the difference between bonding and antibonding states becomes smaller. Therefore when an exciton is composed of a pair of bonding and antibonding states, which is common in simple molecules, the ESF will be repulsive.

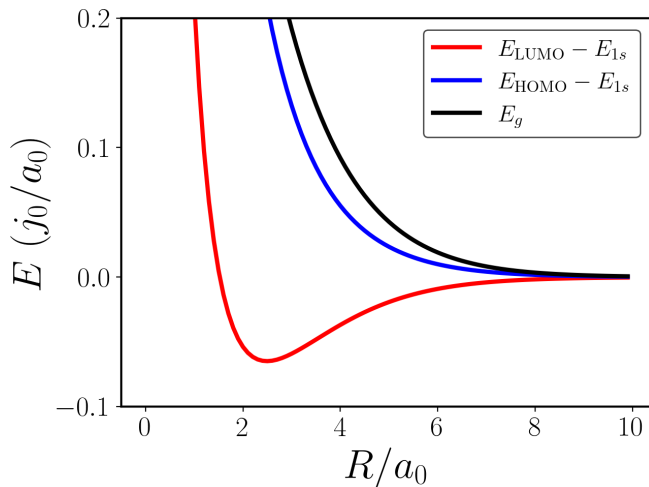


**Figure 20:** HOMO, LUMO and gap energies in a  $H_2^+$  molecule using a tight binding model.

## X. SUPPLEMENTAL MATERIAL

### A. Test calculations for CO molecule

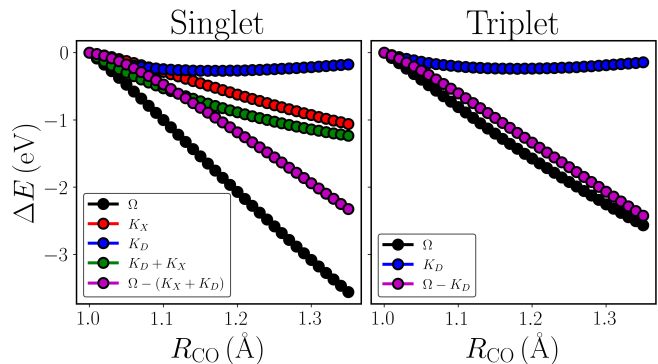


**Figure 21:** Excitation energy, kernel expected energies (exchange and direct) variations by changing the CO molecule bond length.

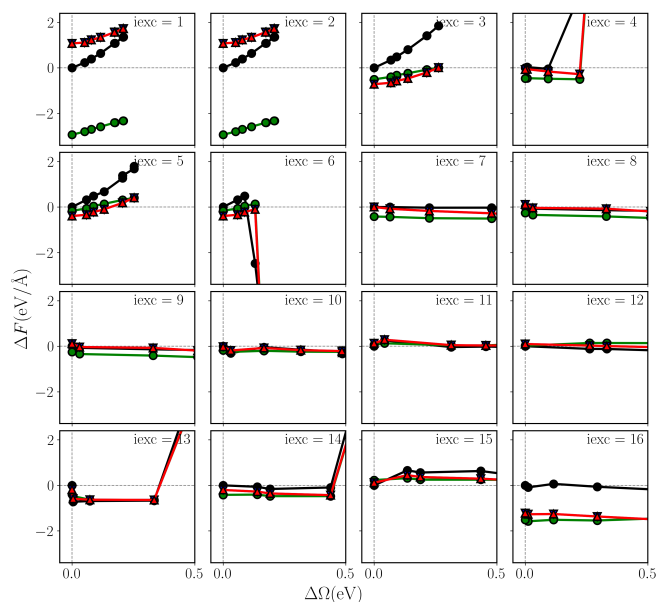


**Figure 22:** Convergence of ESF (y axis) compared with convergence of excitation energies (x axis) for CO. Each point correspond to a BSE and ESF calculations with different number of conduction bands included in the BSE hamiltonian. For some cases the convergence of ESF follows a linear relation with the convergence of excitation energies (for example  $iexc=1$  in this figure), while in other cases the ESF converges faster (for example  $iexc=7$  in this figure). Red triangles correspond to our method, green points correspond to equation 7 and black points corresponds for FD calculations.

Singlet excitation	$R_{CO}$ (pm)
This work	126
Experimental	123.53
TDDFT <sup>87</sup>	122(LDA), 124(PBE), 123(B3LYP)
CIS <sup>87</sup>	118
GW-BSE <sup>69</sup>	126
TDDFT <sup>62</sup>	122
G <sub>0</sub> W <sub>0</sub> /BSE <sup>40</sup>	124.1 (full BSE / FF)
G <sub>0</sub> W <sub>0</sub> /BSE <sup>40</sup>	124.9 (full BSE/ PPM)
G <sub>0</sub> W <sub>0</sub> /BSE <sup>40</sup>	124.9 (TDA / FF)
G <sub>0</sub> W <sub>0</sub> /BSE <sup>40</sup>	125.6 (TDA / PPM)
Triplet excitation	
This work	121
Experimental	120.574
TDDFT <sup>87</sup>	120(LDA), 121(PBE), 120(B3LYP)
CIS <sup>87</sup>	121

**Table I:** Equilibrium bond length for triplet and singlet excited states of CO molecule. CIS stands to single-excitation configuration interaction

- \* Electronic address: rdelgrande@ucmerced.edu
- <sup>1</sup> G. Cohen, J. B. Haber, J. B. Neaton, D. Y. Qiu, and S. Refaely-Abramson, *Phys. Rev. Lett.* **132**, 126902 (2024).
  - <sup>2</sup> Y.-h. Chan, J. B. Haber, M. H. Naik, J. B. Neaton, D. Y. Qiu, F. H. da Jornada, and S. G. Louie, *Nano Lett.* **23**, 3971–3977 (2023).
  - <sup>3</sup> A. M. Alvertis, J. B. Haber, E. A. Engel, S. Sharifzadeh, and J. B. Neaton, *Phys. Rev. Lett.* **130**, 086401 (2023).
  - <sup>4</sup> A. M. Alvertis, R. Pandya, L. A. Muscarella, N. Sawhney, M. Nguyen, B. Ehrler, A. Rao, R. H. Friend, A. W. Chin, and B. Monserrat, *Phys. Rev. B* **102**, 081122 (2020).
  - <sup>5</sup> X. Jiang, Q. Zheng, Z. Lan, W. A. Saidi, X. Ren, and J. Zhao, *Sci. Adv.* **7**, eabf3759 (2021).
  - <sup>6</sup> Q.-M. Hong, R.-P. Xu, T.-Y. Jin, J.-X. Tang, and Y.-Q. Li, *Org. Elect.* **67**, 19 (2019).
  - <sup>7</sup> A. A. Leonard, B. T. Diroll, N. C. Flanders, S. Panuganti, A. Brumberg, M. S. Kirschner, S. A. Cuthriell, S. M. Harvey, N. E. Watkins, J. Yu, et al., *ACS Nano* **17**, 5306 (2023).
  - <sup>8</sup> X. Wu, L. Z. Tan, X. Shen, T. Hu, K. Miyata, M. T. Trinh, R. Li, R. Coffee, S. Liu, D. A. Egger, et al., *Sci. Adv.* **3**, e1602388 (2017).
  - <sup>9</sup> H. Tsai, R. Asadpour, J.-C. Blancon, C. C. Stoumpos, O. Durand, J. W. Strzalka, B. Chen, R. Verduzco, P. M. Ajayan, S. Tretiak, et al., *Science* **360**, 67 (2018).
  - <sup>10</sup> Y. Lan, X. Tao, X. Kong, Y. He, X. Zheng, M. Sutton, M. G. Kanatzidis, H. Guo, and D. G. Cooke, *J. Chem. Phys.* **151**, 214201 (2019).
  - <sup>11</sup> C. Trovatiello, H. P. C. Miranda, A. Molina-Sánchez, R. Borrego-Varillas, C. Manzoni, L. Moretti, L. Ganzer, M. Maiuri, J. Wang, D. Dumcenco, et al., *ACS Nano* **14**, 5700–5710 (2020).
  - <sup>12</sup> C. J. Sayers, A. Genco, C. Trovatiello, S. D. Conte, V. O. Khaustov, J. Cervantes-Villanueva, D. Sangalli, A. Molina-Sanchez, C. Coletti, C. Gadermaier, et al., *Nano Lett.* **23**, 9235–9242 (2023).
  - <sup>13</sup> D. Li, C. Trovatiello, S. Dal Conte, M. Nuß, G. Soavi, G. Wang, A. C. Ferrari, G. Cerullo, and T. Brixner, *Nat. Comm.* **12** (2021).
  - <sup>14</sup> T. Y. Jeong, B. M. Jin, S. H. Rhim, L. Debbichi, J. Park, Y. D. Jang, H. R. Lee, D.-H. Chae, D. Lee, Y.-H. Kim, et al., *ACS Nano* **10**, 5560–5566 (2016).
  - <sup>15</sup> S. Mor, V. Gosetti, A. Molina-Sánchez, D. Sangalli, S. Achilli, V. F. Agekyan, P. Franceschini, C. Giannetti, L. Sangaletti, and S. Pagliara, *Phys. Rev. Res.* **3** (2021).
  - <sup>16</sup> M. S. Hybertsen and S. G. Louie, *Phys. Rev. B* **34**, 5390 (1986).
  - <sup>17</sup> M. Rohlfing and S. G. Louie, *Phys. Rev. B* **62**, 4927 (2000).
  - <sup>18</sup> F. Paleari, H. P. C. Miranda, A. Molina-Sánchez, and L. Wirtz, *Phys. Rev. Lett.* **122**, 187401 (2019).
  - <sup>19</sup> E. Cannuccia, B. Monserrat, and C. Attacalite, *Phys. Rev. B* **99**, 081109 (2019).
  - <sup>20</sup> T. A. Huang, M. Zacharias, D. K. Lewis, F. Giustino, and S. Sharifzadeh, *J. Phys. Chem. Lett.* **12**, 3802–3808 (2021).
  - <sup>21</sup> S. Shree, M. Semina, C. Robert, B. Han, T. Amand, A. Balocchi, M. Manca, E. Courtade, X. Marie, T. Taniguchi, et al., *Phys. Rev. B* **98**, 035302 (2018).
  - <sup>22</sup> H.-Y. Chen, D. Sangalli, and M. Bernardi, *Phys. Rev. Lett.* **125**, 107401 (2020).
  - <sup>23</sup> G. Antonius and S. G. Louie, *Phys. Rev. B* **105**, 085111 (2022).
  - <sup>24</sup> M. Zanfagnini, A. Plaud, I. Stenger, F. Fossard, L. Sponza, L. Schué, F. Paleari, E. Molinari, D. Varsano, L. Wirtz, et al., *Phys. Rev. Lett.* **131**, 206902 (2023).
  - <sup>25</sup> P. Lechiffart, F. Paleari, D. Sangalli, and C. Attacalite, *Phys. Rev. Mater.* **7**, 024006 (2023).
  - <sup>26</sup> F. Paleari and A. Marini, *Phys. Rev. B* **106**, 125403 (2022).
  - <sup>27</sup> S. Brem, A. Ekman, D. Christiansen, F. Katsch, M. Selig, C. Robert, X. Marie, B. Urbaszek, A. Knorr, and E. Malic, *Nano Lett.* **20**, 2849–2856 (2020).
  - <sup>28</sup> F. Libbi, P. M. M. de Melo, Z. Zanolli, M. J. Verstraete, and N. Marzari, *Phys. Rev. Lett.* **128** (2022).
  - <sup>29</sup> H. Mishra and S. Bhattacharya, *Phys. Rev. B* **99**, 165201 (2019).
  - <sup>30</sup> A. M. Kelley, *J. Chem. Phys.* **151**, 140901 (2019).
  - <sup>31</sup> T. Q. P. Vuong, G. Cassaboies, P. Valvin, S. Liu, J. H. Edgar, and B. Gil, *Phys. Rev. B* **95**, 201202 (2017).
  - <sup>32</sup> S. Reichardt and L. Wirtz, *Sci. Adv.* **6**, eabb5915 (2020).
  - <sup>33</sup> S. Reichardt and L. Wirtz, *Phys. Rev. B* **99**, 174312 (2019).
  - <sup>34</sup> Y. Gillet, S. Kontur, M. Giantomassi, C. Draxl, and X. Gonze, *Sci. Rep.* **7** (2017).
  - <sup>35</sup> Y. Wang, B. R. Carvalho, and V. H. Crespi, *Phys. Rev. B* **98**, 161405 (2018).
  - <sup>36</sup> A. Geondzhian and K. Gilmore, *Phys. Rev. B* **98**, 214305 (2018).
  - <sup>37</sup> A. M. Alvertis, J. B. Haber, Z. Li, C. J. N. Coveney, S. G. Louie, M. R. Filip, and J. B. Neaton, *Proc. Nat. Acad. Sci.* **121**, e2403434121 (2024).
  - <sup>38</sup> M. R. Filip, J. B. Haber, and J. B. Neaton, *Phys. Rev. Lett.* **127**, 067401 (2021).
  - <sup>39</sup> Y. Gillet, M. Giantomassi, and X. Gonze, *Phys. Rev. B* **88**, 094305 (2013).
  - <sup>40</sup> O. Çaylak and B. Baumeier, *J. Chem. Theo. Comp.* **17**, 879 (2021).
  - <sup>41</sup> P. Cudazzo, *Phys. Rev. B* **102**, 045136 (2020).
  - <sup>42</sup> L. Adamska and P. Umari, *Phys. Rev. B* **103**, 075201 (2021).
  - <sup>43</sup> Z. Dai, C. Lian, J. Lafuente-Bartolome, and F. Giustino, *Phys. Rev. B* **109**, 045202 (2024).
  - <sup>44</sup> Z. Dai, C. Lian, J. Lafuente-Bartolome, and F. Giustino, *Phys. Rev. Lett.* **132**, 036902 (2024).
  - <sup>45</sup> W. H. Sio, C. Verdi, S. Poncé, and F. Giustino, *Phys. Rev. B* **99**, 235139 (2019).
  - <sup>46</sup> W. H. Sio, C. Verdi, S. Poncé, and F. Giustino, *Phys. Rev. Lett.* **122**, 246403 (2019).
  - <sup>47</sup> V. Perebeinos, J. Tersoff, and P. Avouris, *Phys. Rev. Lett.* **94**, 027402 (2005).
  - <sup>48</sup> Q. Zheng, W. Chu, C. Zhao, L. Zhang, H. Guo, Y. Wang, X. Jiang, and J. Zhao, *WIREs Computational Molecular Science* **9**, e1411 (2019).
  - <sup>49</sup> X. Wang, W. Meng, W. Liao, J. Wang, R.-G. Xiong, and Y. Yan, *J. Phys. Chem. Lett.* **10**, 501 (2019).
  - <sup>50</sup> J. Luo, X. Wang, S. Li, J. Liu, Y. Guo, G. Niu, L. Yao, Y. Fu, L. Gao, Q. Dong, et al., *Nature* **563**, 541 (2018).
  - <sup>51</sup> S. Ismail-Beigi and S. G. Louie, *Phys. Rev. Lett.* **95**, 156401 (2005).
  - <sup>52</sup> J. Deslippe, G. Samsonidze, D. A. Strubbe, M. Jain, M. L. Cohen, and S. G. Louie, *Comp. Phys. Comm.* **183**, 1269 (2012).
  - <sup>53</sup> M. D. Ben and S. L. Rafael Del Grande, David Strubbe (2024), arXiv.
  - <sup>54</sup> P. Giannozzi, S. Baroni, N. Bonini, M. Calandra, R. Car, C. Cavazzoni, D. Ceresoli, G. L. Chiarotti, M. Cococcioni, I. Dabo, et al., *J. Phys. Cond. Mat.* **21**, 395502 (2009).
  - <sup>55</sup> P. Giannozzi, O. Andreussi, T. Brumme, O. Bunau, M. B. Nardelli, M. Calandra, R. Car, C. Cavazzoni, D. Ceresoli, M. Cococcioni, et al., *J. Phys. Cond. Mat.* **29**, 465901 (2017).
  - <sup>56</sup> P. Giannozzi, O. Baseggio, P. Bonfà, D. Brunato, R. Car, I. Carnimeo, C. Cavazzoni, S. de Gironcoli, P. Delugas, F. Ferrari Ruffino, et al., *J. Chem. Phys.* **152**, 154105 (2020).

- (2020).
- <sup>57</sup> S. Baroni, S. de Gironcoli, A. Dal Corso, and P. Giannozzi, *Rev. Mod. Phys.* **73**, 515 (2001).
- <sup>58</sup> F. Giustino, *Rev. Mod. Phys.* **89**, 015003 (2017).
- <sup>59</sup> T. Tsukagoshi and O. Sugino, *Phys. Rev. A* **86**, 064501 (2012).
- <sup>60</sup> X. Andrade, D. Strubbe, U. De Giovannini, A. H. Larsen, M. J. T. Oliveira, J. Alberdi-Rodriguez, A. Varas, I. Theophilou, N. Helbig, M. J. Verstraete, et al., *Phys. Chem. Chem. Phys.* **17**, 31371 (2015).
- <sup>61</sup> A. Sitt, L. Kronik, S. Ismail-Beigi, and J. R. Chelikowsky, *Phys. Rev. A* **76**, 054501 (2007).
- <sup>62</sup> J. Haruyama, T. Suzuki, C. Hu, and K. Watanabe, *Phys. Rev. A* **85**, 012516 (2012).
- <sup>63</sup> Y. Jin, V. W.-z. Yu, M. Govoni, A. C. Xu, and G. Galli, *J. Chem. Theo. Comp.* **19**, 8689–8705 (2023).
- <sup>64</sup> Y. Jin, M. Rusishvili, M. Govoni, and G. Galli, *J. Phys. Chem. Lett.* **15**, 3229–3237 (2024).
- <sup>65</sup> F. Furche and R. Ahlrichs, *J. Chem. Phys.* **117**, 7433 (2002).
- <sup>66</sup> G. Onida, L. Reining, and A. Rubio, *Rev. Mod. Phys.* **74**, 601 (2002).
- <sup>67</sup> D. Wing, J. B. Haber, R. Noff, B. Barker, D. A. Egger, A. Ramasubramaniam, S. G. Louie, J. B. Neaton, and L. Kronik, *Phys. Rev. Mater.* **3**, 064603 (2019).
- <sup>68</sup> A. Kirchhoff, T. Deilmann, and M. Rohlfing, *Phys. Rev. B* **109**, 085127 (2024).
- <sup>69</sup> S. Ismail-Beigi and S. G. Louie, *Phys. Rev. Lett.* **90**, 076401 (2003).
- <sup>70</sup> J. Villalobos-Castro, I. Knysh, D. Jacquemin, I. Duchemin, and X. Blase, *J. Chem. Phys.* **159** (2023).
- <sup>71</sup> G. Antonius, S. Poncé, P. Boulanger, M. Côté, and X. Gonze, *Phys. Rev. Lett.* **112**, 215501 (2014).
- <sup>72</sup> Z. Li, G. Antonius, M. Wu, F. H. da Jornada, and S. G. Louie, *Phys. Rev. Lett.* **122**, 186402 (2019).
- <sup>73</sup> C. Faber, J. L. Janssen, M. Côté, E. Runge, and X. Blase, *Phys. Rev. B* **84**, 155104 (2011).
- <sup>74</sup> C. Faber, P. Boulanger, C. Attaccalite, E. Cannuccia, I. Duchemin, T. Deutsch, and X. Blase, *Phys. Rev. B* **91**, 155109 (2015).
- <sup>75</sup> D. A. Strubbe, Ph.D. thesis, University of California, Berkeley (2012).
- <sup>76</sup> Z. H. Levine and D. C. Allan, *Phys. Rev. Lett.* **63**, 1719 (1989).
- <sup>77</sup> J. Noffsinger, F. Giustino, B. D. Malone, C.-H. Park, S. G. Louie, and M. L. Cohen, *Comp. Phys. Comm.* **181**, 2140 (2010).
- <sup>78</sup> S. Poncé, E. Margine, C. Verdi, and F. Giustino, *Comp. Phys. Comm.* **209**, 116 (2016).
- <sup>79</sup> H. Lee, S. Poncé, K. Bushick, S. Hajinazar, J. Lafuente-Bartolome, J. Leveillee, C. Lian, J.-M. Lihm, F. Macheda, H. Mori, et al., *npj Comp. Mat.* **9** (2023).
- <sup>80</sup> A. Ambrosetti, P. Umari, P. L. Silvestrelli, J. Elliott, and A. Tkatchenko, *Nat. Comm.* **13** (2022).
- <sup>81</sup> D. Y. Qiu, F. H. da Jornada, and S. G. Louie, *Phys. Rev. B* **103**, 045117 (2021).
- <sup>82</sup> D. Y. Qiu, F. H. da Jornada, and S. G. Louie, *Phys. Rev. B* **93**, 235435 (2016).
- <sup>83</sup> M. van Setten, M. Giantomassi, E. Bousquet, M. Verstraete, D. Hamann, X. Gonze, and G.-M. Rignanese, *Comp. Phys. Comm.* **226**, 39 (2018).
- <sup>84</sup> J. Deslippe, G. Samsonidze, M. Jain, M. L. Cohen, and S. G. Louie, *Phys. Rev. B* **87**, 165124 (2013).
- <sup>85</sup> P. Atkins and R. Friedman, *Molecular Quantum Mechanics* (OUP Oxford, 2011), ISBN 9780199541423.
- <sup>86</sup> NIST, *Nist chemistry webbook, nist standard reference database #69* (2001), accessed: 06-08-2024, URL <http://webbook.nist.gov>.
- <sup>87</sup> J. Liu and W. Z. Liang, *J. Chem. Phys.* **134**, 044114 (2011).
- <sup>88</sup> that depended on  $\partial\epsilon_m/\partial u^\nu$  for the C<sub>60</sub> fullerene molecule, where  $\epsilon_m$  is the three-fold degenerate LUMO energy level calculated with DFT and GW and  $u^\nu$  is the displacement pattern for the  $\nu$  vibrational mode using finite differences. Note that  $\partial\epsilon_m/\partial u^\nu$  can also be rewritten in the notation of our work as  $\langle m|\partial_\nu H|m\rangle$  the diagonal electron-phonon coupling coefficient